

Supporting Information

Highly porous carbons derived from MOFs for shape-stabilized phase change materials with high storage capacity and thermal conductivity

**Jia Tang,^a Ming Yang,^a Wenjun Dong,^{*a} Mu Yang,^a Huan Zhang,^a Shuang Fan,^b
Jun Wang,^b Li Tan,^a and Ge Wang^{*a}**

^a School of Materials Science and Engineering, University of Science and Technology Beijing, Beijing 100083, PR China

^b School of Mechanical Engineering, University of Science and Technology Beijing, Beijing 10083, PR China

Table of Contents:

X-ray diffraction measurements (XRD)	S1-S3
Scanning Electron Microscopy (SEM) and high-resolution transmission electromicroscopy (HRTEM)	S4
Thermogravimetric analyses (TGA)	S5
Differential scanning calorimetry (DSC)	S6- S11
Fourier transform infrared (FT-IR) spectroscopy measurements	S12-S13

X-ray diffraction measurements (XRD)

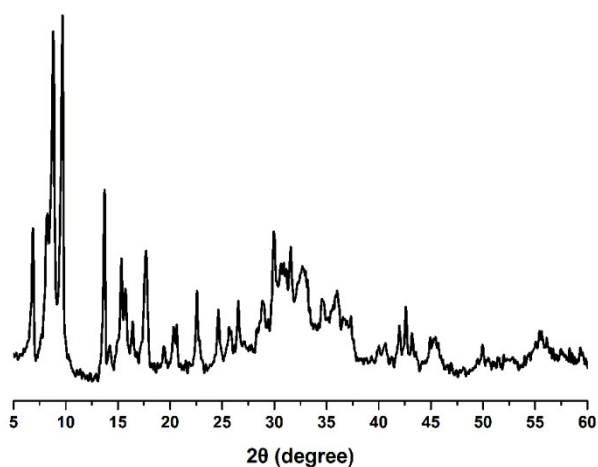


Fig S1. XRD patterns of MOF-5. The synthesis of MOF-5 was carried out according to previously reported procedures.¹ The X-ray diffraction (XRD) result confirms the crystalline structure of the as-prepared MOF-5.²

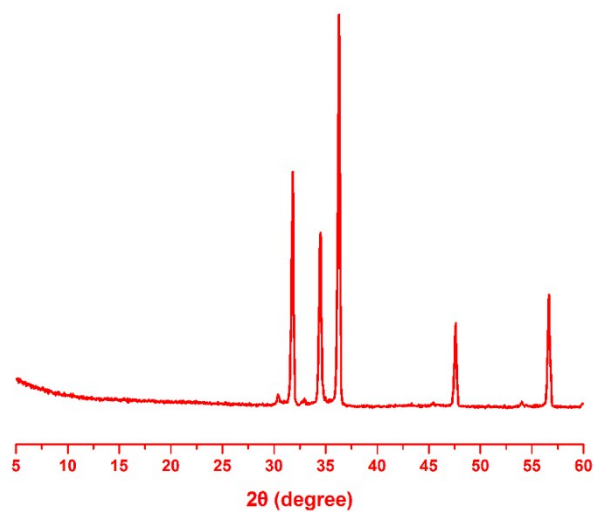


Fig S2. XRD patterns of HPC-900. The HPC-900 was obtained by the direct carbonization of MOF-5. MOF-5 powder in an alumina boat was heated to a target temperature 900 °C at a heating rate of 5 °C min⁻¹ under N₂ flow and maintained for 6 h, and then cooled to room temperature. Only XRD peaks of ZnO could be observed (Fig S2).

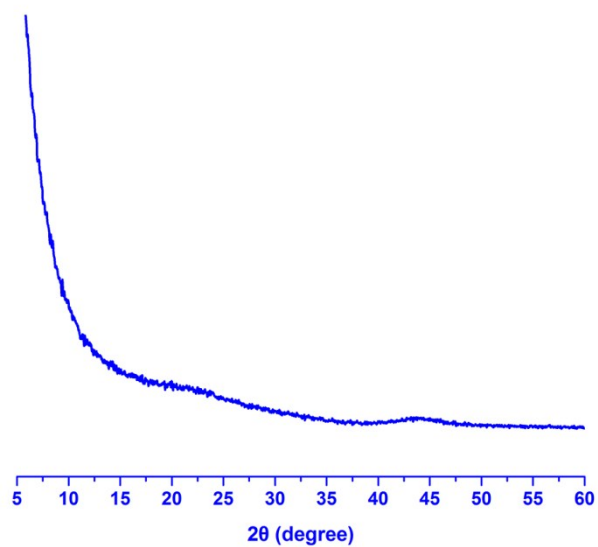


Fig S3. XRD patterns of HPC-1000. The HPC-1000 was obtained by the direct carbonization of MOF-5. MOF-5 powder in an alumina boat was heated to a target temperature 1000 °C at a heating rate of 5 °C min⁻¹ under N₂ flow and maintained for 6 h, and then cooled to room temperature. The weak and broad XRD peaks at ~24° and ~44° indicate the formation of disordered tiny graphitic structure in HPC-1000 carbon (Fig. S3).

Scanning Electron Microscopy (SEM) and high-resolution transmission electromicroscopy (HRTEM)

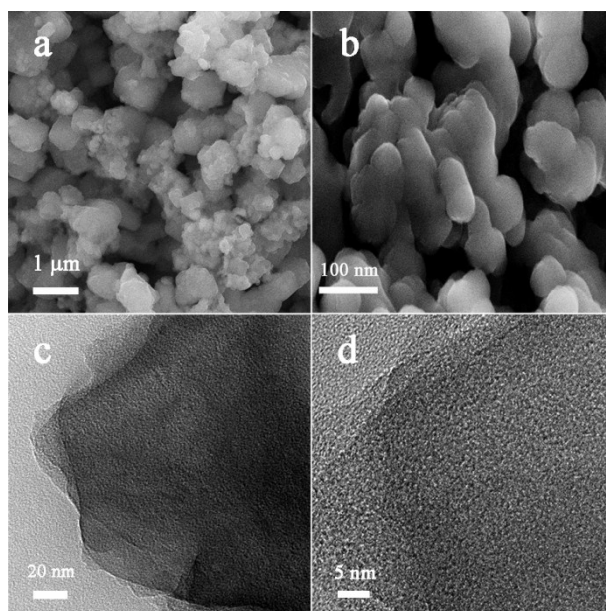


Fig S4. SEM images of (a) MOF-5, (b) HPC-1000 and TEM images of (c-d) HPC-1000. The SEM images show that after the carbonation, HPC-1000 keeps the similar shape to its precursor (Fig. S4a-b). The HRTEM images reveal that almost no ordered graphene layer could be observed (Fig. S4c-d).

Thermogravimetric analyses (TGA)

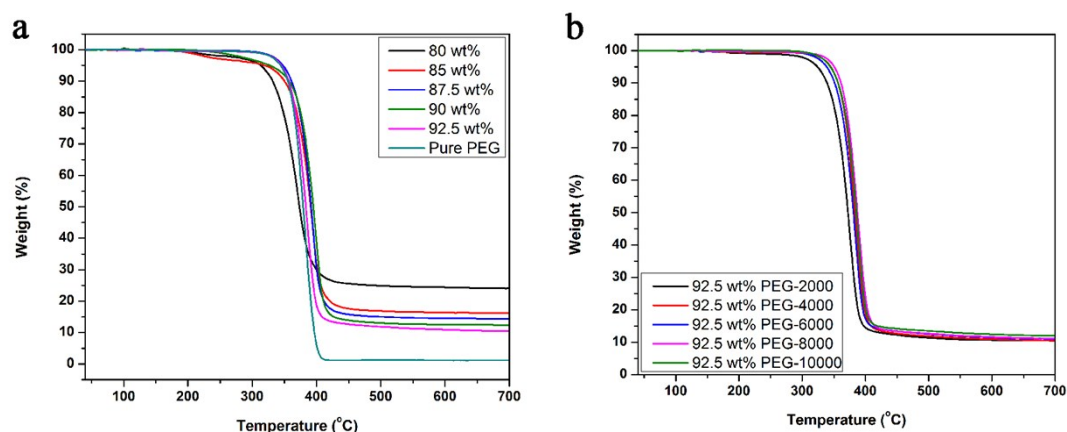


Fig S5. TGA curves of PEG@HPC-1000 PCMs with (a) various PEG-4000 weight percentages and (b) various PEG molecular weights.

Differential scanning calorimetry (DSC)

The PEG@HPC-1000 composite PCMs were characterized in terms of thermal properties by differential scanning calorimetry (DSC) using a NETZSCH STA449F3 (Germany) at 5 °C min⁻¹ heating rate and 5 °C min⁻¹ cooling rate. Samples (5±1 mg) were put into Al₂O₃ pans with covers. Thermal conductivity was measured by a transient plane source technique (TPS), using a hot disk thermal constants analyzer (Hot Disk TPS 2500 S, Hot Disk AB Company, Gothenburg, Sweden). 1g of sample was pressured into tablets with the diameter of 1.3 cm under the pressure of 20 MPa using an oil pump.

Table S1. Thermal properties of the synthesized PEG-4000@HPC-1000 composites with various PEG-4000 weight percentages.

Sample	T _m (°C)	ΔH _m (J/g)	T _c (°C)	ΔH _c (J/g)	Thermal conductivity (W/(m K))
PEG-4000	62.75	164.9	32.34	152.9	0.27
80wt%PEG-4000@HPC-1000	58.80	106.7	33.55	102.2	0.45
85wt%PEG-4000@HPC-1000	59.25	105	34.89	100.7	0.4
87.5wt%PEG-4000@HPC-1000	58.83	138.5	31.11	134.6	0.42
90wt%PEG-4000@HPC-1000	60.24	154.5	31.96	142.6	0.42
92.5wt%PEG-4000@HPC-1000	60.03	162	32.61	161	0.42

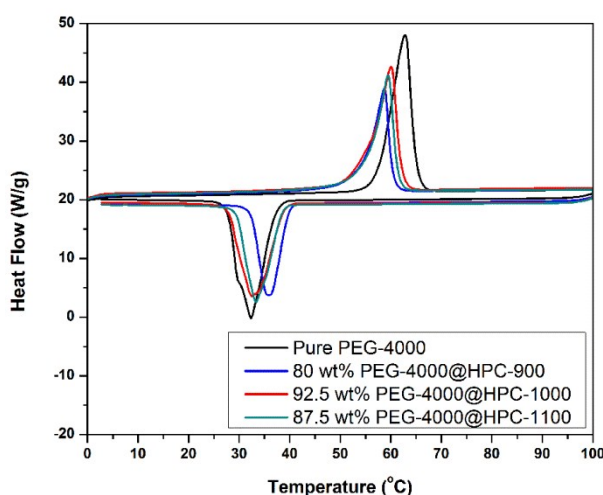


Fig S6. The DSC curves of pure PEG-4000, PEG@HPC-900, PEG@HPC-1000 and PEG@HPC-1100 with the maximum weight percentages of PEG-4000, respectively.

Table S2. Thermal properties of PEG@HPC-900, PEG@HPC-1000 and PEG@HPC-1100 with the maximum weight percentages of PEG-4000, respectively.

Sample	T_m (°C)	ΔH_m (J/g)	T_c (°C)	H_c (J/g)	Thermal conductivity (W/(m K))
PEG-4000	62.75	164.9	32.34	152.9	0.27
80wt%PEG-4000@HPC-900	58.70	105.7	36.09	98.5	0.47
92.5wt%PEG-4000@HPC-1000	60.03	162	32.61	161	0.42
87.5wt%PEG-4000@HPC-1100	59.67	157.2	33.18	152.8	0.42

Table S3. Phase change enthalpies of PEGs, 92.5 wt% PEG@HPC-1000 composite form-stable PCMs with different PEG molecular weights, and their cycling samples, respectively.

Sample	T_m (°C)	ΔH_m (J/g)	T_c (°C)	ΔH_c (J/g)
PEG2000	52.47	154.1	26.22	-139.7
92.5wt%PEG-2000@HPC-1000	53.12	160.4	24.70	157.7
92.5wt%PEG-2000@HPC-1000 50 times cycling	50.30	141.5	21.45	-134.5
PEG4000	62.75	164.9	32.34	-152.9
92.5wt%PEG-4000@HPC-1000	60.03	162.0	32.61	-161.0
92.5wt%PEG-4000@HPC-1000 50 times cycling	57.15	168.1	27.74	-137.1
PEG6000	63.97	173.5	36.52	-160.9
92.5wt%PEG-6000@HPC-1000	60.45	176.0	32.59	-161.7
92.5wt%PEG-6000@HPC-1000 50 times cycling	57.55	166.3	32.99	-144.2

PEG8000	62.74	199	36.90	-195.5
92.5wt%PEG-8000@HPC-1000	61.78	170.8	38.36	-160.7
92.5wt%PEG-8000@HPC-1000 50 times cycling	61.97	163.3	34.78	-147.8
PEG10000	64.49	204.4	38.54	-198.6
92.5wt%PEG-10000@HPC-1000	64.11	181.9	40.18	-170.9
92.5wt%PEG-10000@HPC-1000 50 times cycling	64.45	165.5	37.48	-155.2

Table S4. Thermal conductivity of 92.5 wt% PEG@HPC-1000 composite form-stable PCMs with different PEG molecular weights, respectively.

Sample	Thermal conductivity (W/(m·K))
92.5wt%PEG-2000@HPC-1000	0.43
92.5wt%PEG-4000@HPC-1000	0.42
92.5wt%PEG-6000@HPC-1000	0.40
92.5wt%PEG-8000@HPC-1000	0.42
92.5wt%PEG-10000@HPC-1000	0.39

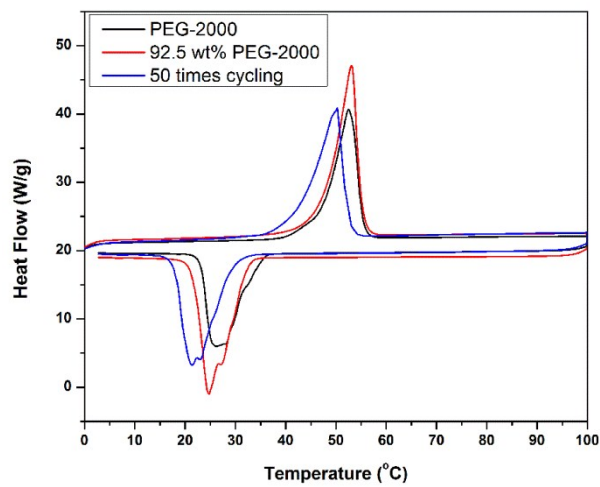


Fig S7. DSC curves of PEG-2000, 92.5wt%PEG-2000 and 50 thermal cycling.

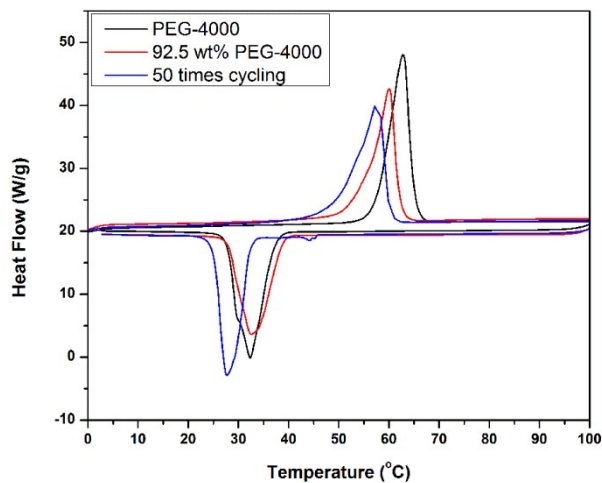


Fig S8. DSC curves of PEG-4000, 92.5wt%PEG-4000 and 50 thermal cycling.

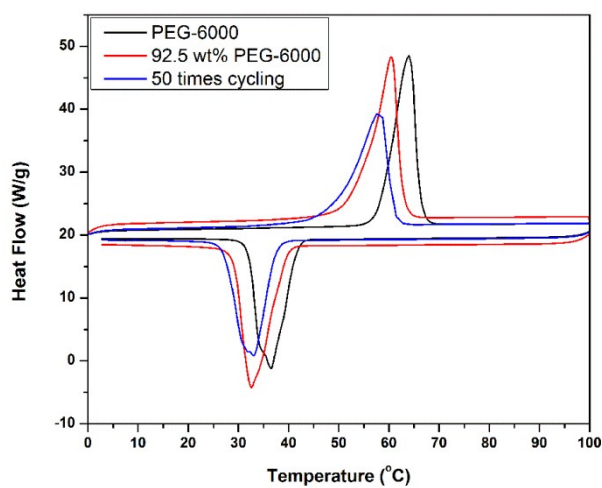


Fig S9. DSC curves of PEG-6000, 92.5wt%PEG-6000 and 50 thermal cycling.

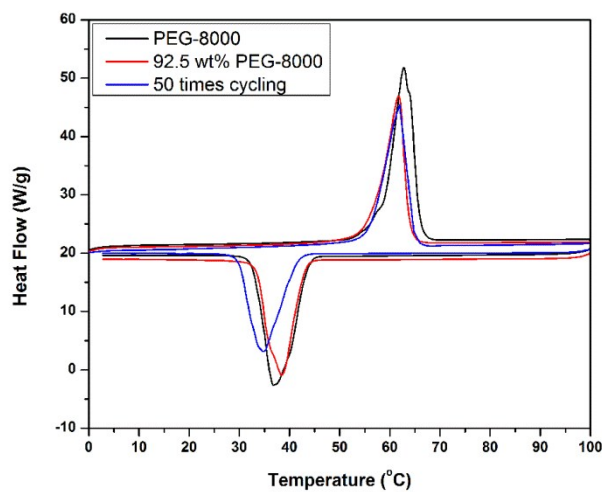


Fig S10. DSC curves of PEG-8000, 92.5wt%PEG-8000 and 50 thermal cycling.

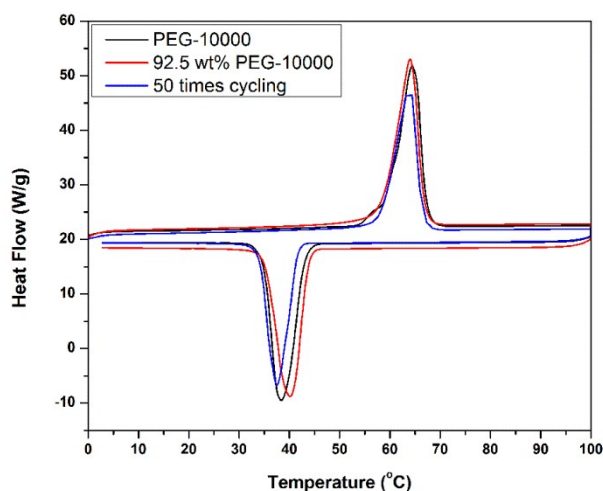


Fig S11. DSC curves of PEG-10000, 92.5wt%PEG-10000 and 50 thermal cycling. The maximum weight percentage of PEG absorbed in the composite PCMs was 92.5 wt% without any leakage. The thermal conductivity of the composite PCMs was about 50%-fold higher than that of pure PEG.

Fourier transform infrared (FT-IR) spectroscopy measurements

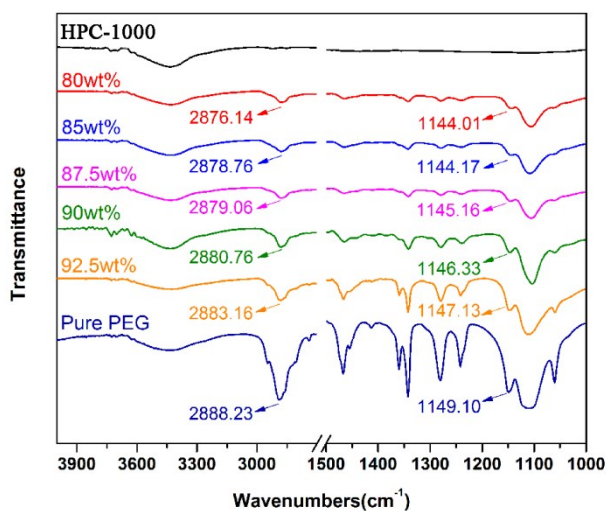


Fig S12. The FTIR spectra of the PEG@HPC-1000 PCMs with various PEG-4000 weight percentages and pure PEG-4000. The peaks corresponding to the stretching vibration of C-H shift from 2888.23 cm^{-1} to 2876.14 cm^{-1} and the frequency shift of the C-O stretching vibration from 1149.10 cm^{-1} to 1144.01 cm^{-1} indicate the interaction between the porous carbon and the H atom of $-\text{CH}_2$ of PEG-4000 (**Fig S13**).³⁻⁴

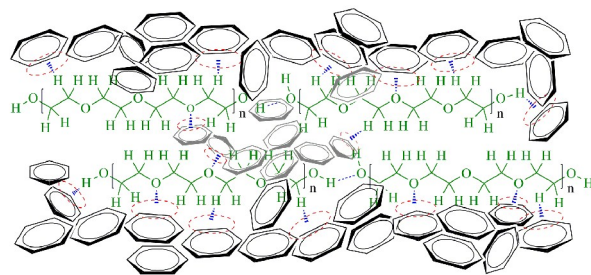


Fig S13. The interaction between HPCs and PEG-4000.

References

1. L. Huang, H. Wang, J. Chen, Z. Wang, J. Sun, D. Zhao, Y. Yan, *Microporous Mesoporous Mater.*, 2003, **58**, 105.
2. G. Srinivas, V. Krungleviciute, Z.X. Guo, T. Yildirim, *Energy. Environ. Sci.*, 2014, **7**, 335.
3. P. Tarakeshwar, H.S. Choi, K.S. Kim, *J. Am. Chem. Soc.*, 2001, **123**, 3323.
4. M. Hu, J. Reboul, S. Furukawa, N.L. Torad, Q. Ji, P. Srinivasu, K. Ariga, S. Kitagawa, Y. Yamauchi, *J. Am. Chem. Soc.*, 2012, **134**, 2864.